



HAL
open science

Alteration of physico-chemical characteristics of coconut endocarp - *Acrocomia aculeata* - by isothermal pyrolysis in the range 250–550 °C

Shirley Duarte, Pin Lv, Giana Almeida, Juan Carlos Rolón, Patrick Perre

► To cite this version:

Shirley Duarte, Pin Lv, Giana Almeida, Juan Carlos Rolón, Patrick Perre. Alteration of physico-chemical characteristics of coconut endocarp - *Acrocomia aculeata* - by isothermal pyrolysis in the range 250–550 °C. *Journal of Analytical and Applied Pyrolysis*, 2017, 126, pp.88-98. 10.1016/j.jaap.2017.06.021 . hal-01652581

HAL Id: hal-01652581

<https://centralesupelec.hal.science/hal-01652581>

Submitted on 1 Dec 2017

HAL is a multi-disciplinary open access archive for the deposit and dissemination of scientific research documents, whether they are published or not. The documents may come from teaching and research institutions in France or abroad, or from public or private research centers.

L'archive ouverte pluridisciplinaire **HAL**, est destinée au dépôt et à la diffusion de documents scientifiques de niveau recherche, publiés ou non, émanant des établissements d'enseignement et de recherche français ou étrangers, des laboratoires publics ou privés.

Alteration of physico-chemical characteristics of coconut endocarp —*Acrocomia aculeata*— by isothermal pyrolysis in the range 250 to 550 °C

Shirley Duarte^{a,c,*}, Pin Lv^b, Giana Almeida^d, Juan Carlos Rolón^{e,f}, Patrick Perré^{a,b}

^a*LGPM, CentraleSupélec, Université Paris-Saclay, Plateau du Moulon, 91190 Gif-sur-Yvette, France*

^b*LGPM, CentraleSupélec, Centre Européen de Biotechnologie et de Bioéconomie (CEBB), 3, rue des Rouges Terres, 51110 Pomacle, France*

^c*Facultad de Ciencias Químicas, Universidad Nacional de Asunción, San Lorenzo, 2160, Paraguay.*

^d*UMR GENIAL, AgroParisTech, INRA, Université Paris-Saclay, 91300 Massy, France*

^e*Facultad de Ingeniería, Universidad Nacional de Asunción, San Lorenzo, 2160, Paraguay*

^f*Visiting professor at LGPM, Centrale-Supélec, Châtenay-Malabry, 92290, France*

Abstract

Characteristics of the endocarp of *Acrocomia aculeata* fruit samples were evaluated before and after 2 h of isothermal pyrolysis in the range 250 to 550 °C. Differential thermogravimetric (DTG) curves from the char, obtained at 300 °C, confirm that degradation of hemicellulose and cellulose was complete and resulted in approximately 42.5% oxygen loss. The micrographs obtained from scanning electron microscopy with a field emission gun (SEM/FEG) confirmed a softened phase from the chars treated at 250 °C. The van Krevelen analysis shows that energy intensification of the sample transferred from peat to charcoal as the treatment intensity increased; this resulted in a 71% mass loss at 550 °C. The surface area of the treated sample increased exponentially with a factor of 1.2 per percentage of mass loss, from 450 °C and reached 216 m²/g at 550 °C as a consequence of the development of microporous structures. The water-vapor-sorption properties were strongly affected by the treatment, with a pronounced type V isotherm curve for the

*Corresponding author.

Email address: sjoamduart@gmail.com (Shirley Duarte)

char at 550 °C. These results show the evolution in chemical and structural properties of coconut endocarp during its isothermal pyrolysis. In particular, the improved char properties indicate that this material may be used as solid fuel or as raw material for the gasification process.

Keywords: surface area, elemental analysis, dynamic vapor sorption, coconut endocarp, pyrolysis mechanism.

1 Introduction

The South-American palm species *Acrocomia aculeata*, commonly known as mbocayá, macaw, macauba or just coconut palm, has attracted the attention of researchers in recent years, mainly for its enormous potential as a sustainable source of feedstock for biorefinery [1, 2, 3, 4].

Although *Acrocomia aculeata* is a native species of South America, its distribution spans the tropics and subtropics of Mexico and Central America as well. *Acrocomia aculeata* grows in regions that extend from Mexico to Argentina, but only in Paraguay, where 23 palm species have been identified [5], is its fruit (coconut) used commercially [6]; its many potential uses are shown in Fig. 1.

The endocarp represents about 21% of the overall residue mass generated after processing the mbocayá fruit [1]. In addition, it has higher values of fixed carbon, lignin content and energy density than other parts of the fruit [1, 7]. These characteristic properties allow us to consider endocarp as potential feedstock to produce biofuel or materials like charcoal and activated carbon for a variety of applications; the thermochemical conversions, pyrolysis and gasification, could be promising methods to accomplish this.

During pyrolysis, thermal decomposition of biomass components (cellulose, hemicellulose and lignin) takes place. In general, the char produced is expected to have higher carbon content and heating value. Its chemical structure and physical properties such as density, specific surface area, water content, and electrical conduction, changes according to the pyrolysis conditions and feedstocks [8, 9, 10].

The characteristic properties of char indicate its different uses. Some important aspects that make it suitable as a solid fuel, adsorbent or as catalyst, are its hygroscopicity and specified surface area. When planning to use the char in a gasification process, in particular to obtain activated carbon or syn-gas, its porosity, moisture content and chemical composition, are impor-

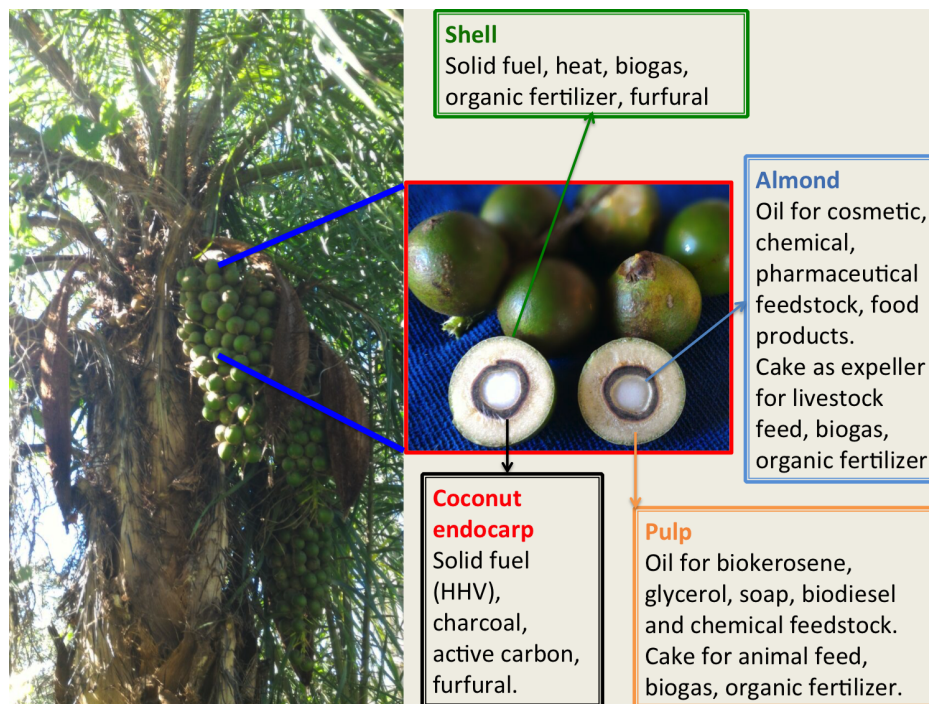


Figure 1: Potential uses of Acrocomia fruit.

30 tant characteristics that result from the process, to maximize a particular
31 product.

32 Adsorption experiments are considered a powerful tool to study materials.
33 In previous studies [11, 12], sorption properties were evaluated in torrefied
34 biomass and bio-char obtained from wood samples. Natural fibers have dis-
35 played differences in water vapor sorption behavior while the hysteresis loop
36 and its lignin contents exhibit a direct relationship [13]. New analysis has
37 also found that a function of the elemental composition in mildly heat-treated
38 wood can predict the occupancy of water sorption sites [14].

39 Though some char properties have been extensively studied [9, 10], to
40 our knowledge, no study concerning the evolution of elemental analysis, sur-
41 face area and water vapor sorption properties during pyrolysis of coconut
42 endocarp, exists.

43 The important role of biomass feedstock in the pyrolysis process is well
44 known. The composition and physical properties of the pyrolysis products
45 depends on the raw material properties. Holocellulose and lignin content in

46 coconut endocarp, was determined by [1, 2] and the intense lignification of
47 its sclereids cells, provides its impermeability and petrous consistency [2, 15].

48 In order to produce different fuels and chemicals from pyrolysis, the com-
49 position of raw material and thermal decomposition mechanism should be
50 determined. Although there are extensive studies on the mechanisms of
51 biomass pyrolysis [16, 17, 18], none is specific to this feedstock or the kinetic
52 progress of its thermal decomposition.

53 In this study, mass loss as a function of time, in static conditions, were
54 used to explain kinetic pyrolysis in the coconut endocarp. Three decom-
55 position rates were observed from the mass loss vs time curves, related to
56 the three main components' degradation. These measurements serves as the
57 basis for future work in developing a kinetic model for biomasses of this type.

58 The major focus of this study is the experimental characterization of
59 the coconut endocarp and its chars, obtained from a variety of isothermal
60 pyrolysis conditions. It is important to propose the more relevant use of
61 coconut endocarp and its chars, as *Acrocomia aculeata* is a potential feedstock
62 for a biorefinery, likely to reduce deforestation and pollution.

63 The analysis techniques employed for this study included: elemental anal-
64 ysis, gas sorption analysis, water vapor sorption analysis, environmental and
65 scanning electron microscopy (ESEM-FEG/SEM). In addition, the thermo-
66 gravimetric TG and DTG curves, for the coconut endocarp and char samples
67 were used as a tool for obtaining information about the main structural com-
68 ponents degradation. From our results, coconut endocarps could be used as
69 feedstock to produce three different products: high-quality bio-oil or solid
70 fuel (treatment at 250 °C to 300 °C), charcoal of different quality depend-
71 ing upon the end use (treatment at 350 °C to 450 °C), and feedstock to a
72 gasification process (treatment above 500 °C).

73 **2. Experimental**

74 *2.1. Materials and pyrolysis conditions*

75 *Acrocomia aculeata*, indigenous to Paraguay, is usually found in areas
76 situated between the latitudes 19 and 27 south and longitudes 54 and 62 west.
77 The solid and woody residue inside the *Acrocomia aculeata* fruit, referred
78 to as ‘coconut endocarp’, was used in this study. The availability of the
79 coconut endocarp, as agroindustrial waste in Paraguay, is about 7 tonnes of
80 dry matter per hectare per year [19]. The feedstock was cleaned with water

81 and dried in air flow at room temperature. Sample particles, between 0.2-
82 0.63 mm selected from a previous work [7], were obtained using a grinder
83 (IKA M20 Universal mill) and subsequently sieved.

84 The pyrolysis was carried out by a STA 449 F3 Jupiter, NETZSCH at
85 atmospheric pressure. Each sample with an initial weigh of 10 ± 2 mg was
86 placed in an alumina crucible and heated at $5 \text{ }^\circ\text{C min}^{-1}$ under a nitrogen
87 flow of 50 mL min^{-1} (STP). Initially, samples were heated from ambient
88 temperature to $100 \text{ }^\circ\text{C}$, and dried for 30 minutes. The temperature was then
89 increased to a final temperature ($250 \text{ }^\circ\text{C}$, $300 \text{ }^\circ\text{C}$, $350 \text{ }^\circ\text{C}$, $400 \text{ }^\circ\text{C}$, $450 \text{ }^\circ\text{C}$,
90 $500 \text{ }^\circ\text{C}$, $550 \text{ }^\circ\text{C}$) and was observed, thereafter, for 2 hours.

91 The percentage mass loss “ ml ” defined as the instantaneous anhydrous
92 mass loss as a function of time, was calculated with the following equation
93 1.

$$ml = \frac{m_i - m_t}{m_i} \times 100 \quad (1)$$

94 where m_i is the anhydrous mass at the beginning of the thermal degra-
95 dation (after they were dried at $100 \text{ }^\circ\text{C}$ for 30 min) and m_t is the anhydrous
96 mass of the char residue (thermal treated sample) in the instant t of the
97 thermal degradation. The final mass loss “ fml ” is measured at the end of
98 the plateau for each selected temperature. This method was employed fol-
99 lowing previous testing in this lab which indicated that 30 min at $100 \text{ }^\circ\text{C}$ was
100 enough time to release the moisture content in powder wood samples [20].

101 The term “char” in this study, refers to the solid residue that remains in
102 the crucible after each treatment. This term, and its associated temperature,
103 are used to refer to the char obtained after each pyrolysis treatment obtained
104 at a specific temperature, for example, “ $350 \text{ }^\circ\text{C}$ -char”, represents the char
105 obtained after the pyrolysis of coconut endocarp at $350 \text{ }^\circ\text{C}$ for 2 h in the
106 condition described above.

107 In addition, derivative thermogravimetric (DTG) curves were plotted for
108 the cases of untreated endocarp and char samples in order to check for
109 the characteristic DTG peaks normally found in carbohydrate decomposi-
110 tion (cellulose, hemicellulose and lignin). The heating rate employed was 10
111 $^\circ\text{C}/\text{min}$ under the nitrogen gas flow of $50 \text{ ml}/\text{min}$. The initial mass sample
112 remained between 3 and 4 mg. All experiments were performed in triplicate
113 and several blank tests were made to correct the effects of buoyancy forces.

114 *2.2. Analytical Methods*

115 *2.2.1. Elemental analysis*

116 The evolution of the elemental composition was measured by Thermo
117 Scientific FLASH 2000 CHNS/O analyzers. In order to determine carbon,
118 hydrogen, nitrogen and sulfur (CHNS), the standard reactants were used:
119 BBOT (2,5-(Bis(5-tert-butyl-2-benzo-oxazol-2-yl) thiophene), methionine, and
120 cysteine. Additionally, vanadium oxide (V_2O_5) was added in order to ensure
121 good resolution of the peaks. BBOT and benzoic acid were used to deter-
122 mine the oxygen (O) content. All the samples were dried at 103 ± 2 °C and
123 stored in a desiccator until the analysis and the experiments were performed
124 in triplicate.

125 Since lignocellulosic biomass are composed of three main chemical com-
126 ponents (cellulose, hemicellulose, lignin), a review of its elemental and prox-
127 imate analyses is shown in Table 1 for comparison proposes.

128 *2.2.2. Surface area BET analysis and porosity characteristics*

129 The surface area evolution of the samples was evaluated by the adsorption
130 of nitrogen at 77 K in the Micromeritics 3Flex surface characterization ana-
131 lyzer. Prior to analysis, the samples were outgassed at 80 °C until achieving
132 a residual pressure of 10^{-4} mmHg, which lasted for different periods of time
133 according to the surface area of each sample. BET surface area, from the
134 isotherms, was calculated using the Brunauer-Emmett-Teller (BET) equa-
135 tion. The relative pressure (P/P_0) range that was considered was 0.01 to
136 0.30 and was assumed to be 0.162 nm^2 , which is the cross-sectional area
137 for a nitrogen molecule. The total mass of the samples used was enough to
138 achieve a good isotherm plot without mathematical smoothing. The pore
139 size distribution was calculated using the Density Functional Theory (DFT)
140 and the total pore volumes were determined from a single adsorption point
141 at a relative pressure $P/P_0 \geq 0.95$. The experiments were performed in
142 triplicate.

143 *2.2.3. Environmental scanning electron microscopy (ESEM) and scanning*
144 *electron microscopy with a field emission gun (SEM-FEG)*

145 Two microscopy analyses were conducted. First, particles (2 mm size),
146 before and after the treatment at 250 °C and 550 °C were evaluated us-
147 ing a FEI Quanta 200 to observe the global changes, under low vacuum,
148 at 0.6 Torr and 12.5 kV. Second, the char residues were recovered from the
149 thermo-gravimetric devices with tungsten and observed, using the Leo 1530

Table 1: Elemental and proximate analyses of the main components of biomasses

components	Ref. ^a	elemental analysis (%wt)			proximate analysis (%wt)		
		C	H	O	Ash	VM ^b	FC ^c
Cellulose		44.4	5.8	49.3	0	94.8	5.2
	[21]	44.5	5.6	49.5	0	94.1	5.9
	[22]	39.99	5.8	54.2	0.51	98.7	0.8
	[23]	42.06	6.06	46.38	-	89.20	5.30
Hemicellulose		46.7	5.7	47.4	4.1	73.3	22.6
	[21]	44.3	5.4	49.9	4.8	75.3	19.9
		44.8	5.6	49.5	10.1	71.1	18.8
Lignin		56.6	4.2	37.1	10	49.9	40.1
	[21]	65	4.9	28.7	13.5	45	41.5
		66.7	5.6	26.1	2.4	58.9	38.7
	[22]	49.53	4.39	46.07	1.71	93.8	4.5
	[23]	47.65	4.30	19.60	12.35	35.74	38.81
	[24]	66.5	5.8	25.3	5.7	-	-

^aDifferences between the results presented by each author, are attributed to different extraction methods and the origin of raw material

^bVolatile matters

^cFixed carbon

150 (SEM-FEG) at 2.00 kV and high vacuum, in order to see the main morpho-
151 logical changes in the cellular wall.

152

153 2.2.4. Water vapor sorption properties of untreated (control) and treated 154 samples

155 Sorption isotherms and hysteresis were measured using a dynamic vapor
156 sorption apparatus (DVS; Surface Measurement Systems Ltd, London, UK)
157 at a temperature of 25 °C. Detailed information about the apparatus can be
158 found in [25]. All of the samples had similar weights 22.2 ± 0.6 mg and were
159 weighed using a sample pan and a micro-balance, which measured the change
160 in the mass under dry nitrogen. The relative humidity (RH) was increased
161 from 0 to 90% in 10% increments. The RH was raised to the next step when
162 the change in sample mass was below $0.002\% \text{ min}^{-1}$ and remained so for
163 10 min. After a constant mass was achieved at 90%, the RH was lowered
164 back to zero in the same configuration as each step. Absolute hysteresis was
165 calculated as the difference between the equilibrium moisture content (EMC)
166 during the desorption ($EMC_{desorption}$) and adsorption ($EMC_{adsorption}$) [26].
167 The experiments were performed in triplicate.

168 3. Results and discussion

169 The aim of this study is to analytically evaluate and correlate the struc-
170 tural and morphological changes in the coconut endocarp with the mass loss
171 produced by the thermal treatment by using physicochemical evolution to
172 explain and to predict these changes.

173

174 3.1. Mass change profile as a function of time

175 When biomass is pyrolyzed, different depolymerization and devolatiliza-
176 tion reactions take place from the polysaccharides and organic polymers de-
177 composition. Anhydrous mass loss during pyrolysis is a consequence of these
178 decompositions and is depicted in Fig. 2.

179 We can clearly observe three behaviors, which are related to the three
180 main components degradation. The first behavior occurs during the treat-
181 ment at 250 °C, with a “*fml*” of about 25%. For this level of temperature,
182 the decomposition of hemicellulose and the release of high-volatility com-
183 pounds and gases (majorly: H_2O , CO , CO_2 and acid compounds) is expected
184 [27, 28].

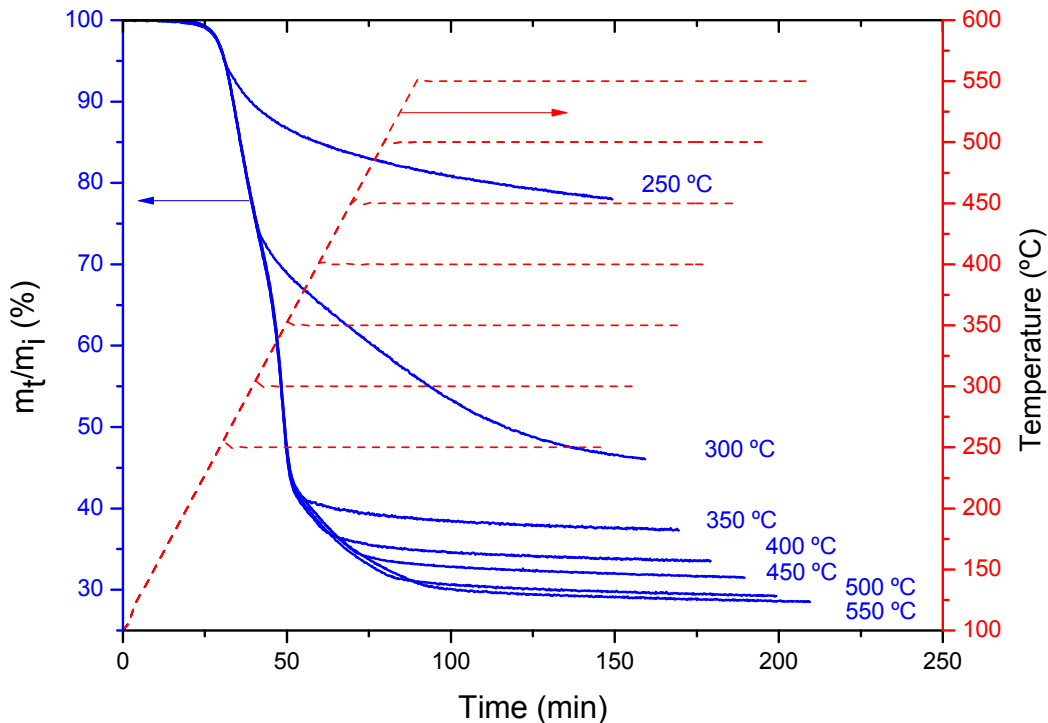


Figure 2: Anhydrous mass loss of coconut endocarp, as a function of time, for each pyrolysis treatment. The red lines indicate the temperature evolution as function of time.

185 The second behavior is observed in the sample treated at 300 °C. It is
 186 mainly the consequence of both hemicellulose and cellulose thermal decom-
 187 position. Cellulose degradation is usually explained as a two-step process: an
 188 initial reaction step that leads to the formation of “active cellulose”, which
 189 then undergoes some competitive reactions that produce char plus perma-
 190 nent gases and volatiles (tar) [29, 30, 31]. It is well known that from 300 to
 191 400 °C, cellulose thermal decomposition occurs with a higher decomposition
 192 rate than lignin, which decomposes in a wide temperature range (250-500
 193 °C) [32, 33]. The slope in the TG curve, nevertheless exhibits a significant
 194 decrease at 350 °C, indicating perhaps, that cellulose has been completely
 195 degraded at this temperature level.

196 The third observed behavior occurs from 350 °C until 550 °C, where the
 197 increment in fml was only 19% of the fml observed until 350 °C. This
 198 behavior is expected because from 350 °C, the main components in the char
 199 residue should be lignin and the degradation solid products derived from

200 the carbohydrates decomposition. This slow mass decrease was observed in
 201 woody biomass [22, 34] as a second stage due the lignin decomposition.

202 Figure 3 illustrates the DTG curves for untreated and char samples. DTG
 203 of coconut endocarp shows two well-defined peaks with a maximum mass-loss
 204 rate of $4.84 \text{ \%wt min}^{-1}$ at $293 \text{ }^\circ\text{C}$ for the hemicellulose and $9.53 \text{ \%wt min}^{-1}$
 205 at $365 \text{ }^\circ\text{C}$ for cellulose decomposition.

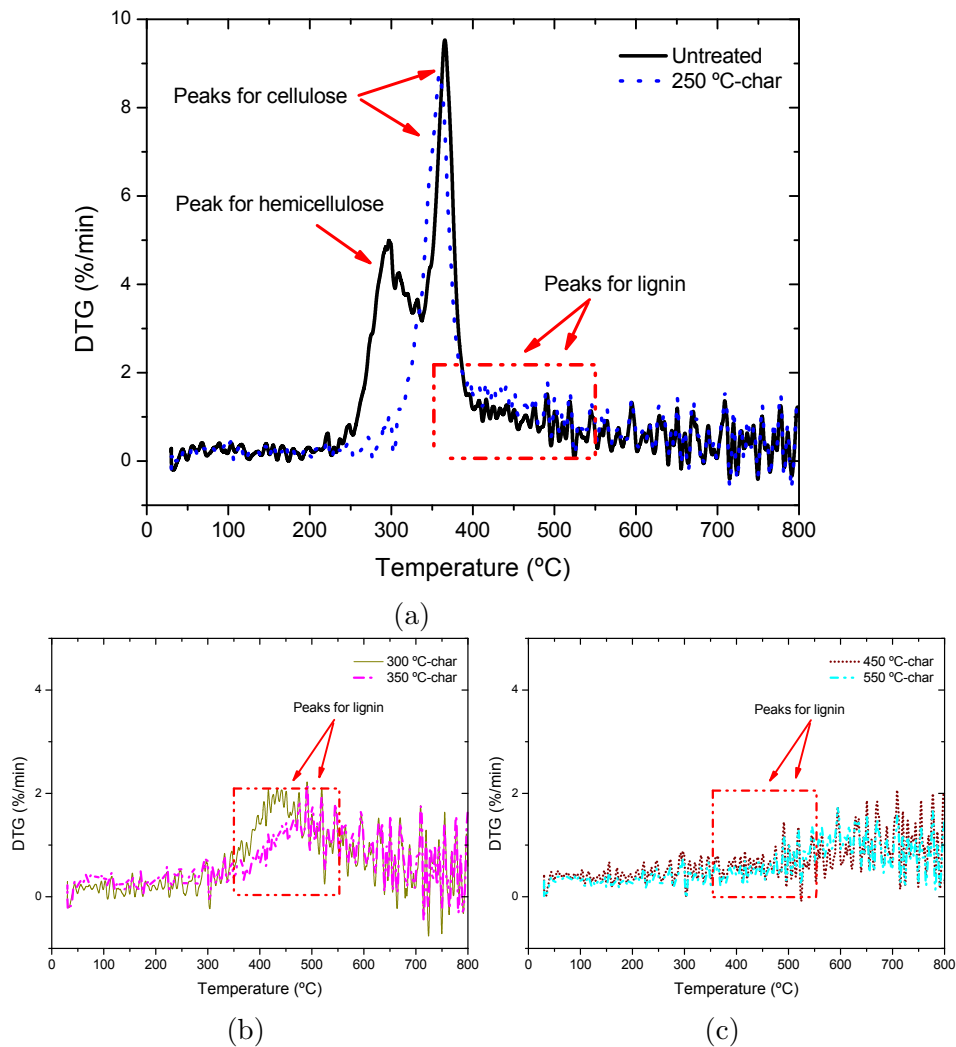


Figure 3: Comparison of DTG curves for (a) untreated and $250 \text{ }^\circ\text{C}$ -char, (b) $300 \text{ }^\circ\text{C}$ -char and $350 \text{ }^\circ\text{C}$ -char, and (c) $450 \text{ }^\circ\text{C}$ -char and $550 \text{ }^\circ\text{C}$ -char.

206 This double-peak was already observed for lignocellulosic biomass with

207 high lignin contents, such as coconut endocarp (*C. nucifera*) [35, 36]. These
208 authors also explained this double peak by high S/G ratios¹. Therefore, we
209 expect similar S/G ratio and the presence of p-hydroxybenzoates, proposed as
210 authentic lignin precursors by [37], for our coconut endocarp lignin structure
211 and composition as presented in [35]. However, the S/G ratios for the isolated
212 lignin of coconut endocarp (*C. nucifera*) exhibits different values. These
213 discrepancies could be due the extraction techniques employed [35, 38].

214 All other peaks, such as hemicellulose and cellulose peaks, were not well-
215 separated in other lignocellulose biomass [32, 39, 40]. A little characteristic
216 shoulder between 350 and 550 °C for lignin which apparently continues until
217 900 °C according to [34], showed a very slow mass loss that reached 1.40 %wt
218 min^{-1} at 416 °C maximum.

219 DTG curves for 250 °C-char also depicts the sharp and shoulder peaks
220 for cellulose and lignin, respectively. But the 300 °C-char, exhibited only the
221 characteristic shoulder for lignin on the DTG curve, which indicated that
222 the degradation of cellulose and hemicellulose were completed. This led us
223 to suppose that at most 54 %wt of the coconut endocarp is composed of
224 holocellulose, considering that the lignin decomposed slower than the other
225 components, which is also in accordance with the results presented in [41].

226 The same shoulder, but at higher temperatures (550 °C), appears for
227 350 °C-char DTG curve. As lignin is resilient to pyrolysis, its relative con-
228 tent increases with pyrolysis temperature at similar residence time. So, as
229 suggested in [36] higher lignin content can be expected for higher pyrolysis
230 temperatures.

231 In the chars treated at 450 and 550 °C, this marking shoulder has appar-
232 ently disappeared.

233 Mass loss results from numerous competitive reactions and this thermo-
234 gravimetric curves can give us insight about the reaction mechanisms for the
235 coconut endocarp pyrolysis.

236

237 3.2. Elemental composition

238 Elemental and surface analyses for the untreated and char samples are
239 given in Table 2. Note that sulfur was not detected in any sample.

¹syringyl- and guaiacyl- lignin units ratio

Table 2: Elemental composition and physical properties for untreated and char samples

	<i>fml</i> (%wt)	elemental analysis (%wt) ^a					surface area BET (m^2/g)	total pores volume (cc/g) $\times 10^{-3}$	micropore volume (cc/g) $\times 10^{-3}$
		C	H	N	O	S			
Untreated	—	51.1	5.53	0.37	42.6	0.00	0.28	0.603	0.014
250 °C-char	22.0	56.9	4.95	0.40	38.6	0.00	0.30	0.322	0.079
300 °C-char	53.9	68.9	4.11	0.25	24.5	0.00	0.44	0.439	0.108
350 °C-char	62.7	71.9	3.75	0.26	21.1	0.00	0.52	0.457	0.138
400 °C-char	66.5	75.1	3.34	0.27	18.1	0.00	0.57	0.520	0.175
450 °C-char	68.5	78.2	3.02	0.28	13.6	0.00	5.95	2.56	2.06
500 °C-char	70.7	82.1	2.78	0.31	9.10	0.00	108	45.7	42.3
550 °C-char	71.5	85.7	2.55	0.59	6.08	0.00	216	89.1	84.2

^aFor an analyzer detection limit of 0.01% (100 ppm).

240 Coconut endocarp has a high lignin composition with amounts of carbon
241 (C) higher than 50% and oxygen (O) lower than 43%, in comparison to values
242 reported in Table 1. These results are expected since the coconut endocarp
243 has in average a high lignin content of approximately 35% and hollocelulose
244 content of approximately 53% [1, 41].

245 Another important observation is that the sum (C + H + N + O) is
246 not equal to 100% from 300 °C-char. This is due to char fraction contains
247 inorganic materials (ash) and its proportion increases with the pyrolysis tem-
248 perature [42, 43].

249 The most important thermochemical reactions can be visualized from the
250 van Krevelen diagram (Fig. 4a). Overall, dehydration and decarboxylation
251 reactions, led coconut endocarp to become more lignin-like, even from the
252 first treatment at 250 °C.

253 Notable oxygen reduction from the initial oxygen content occurs for the
254 sample treated at 300 °C ($\approx 24\%$), which is expected from the hemicellulose
255 and cellulose decomposition and the devolatilization of low molecular mass
256 products at this temperature.

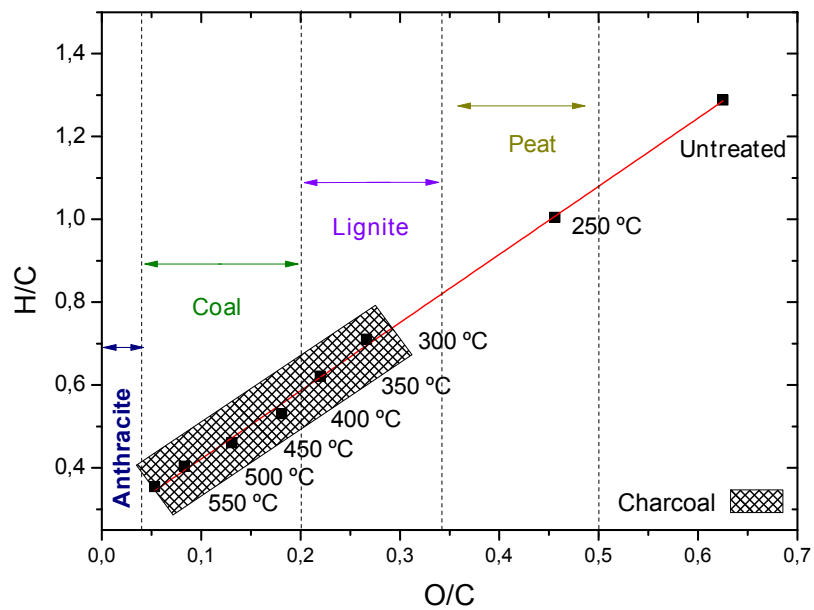
257 Considering the oxygen reduction, the low sulfur content and the lignin-
258 like characteristic of char obtained at 250 °C and 300 °C, an interesting
259 output could be the production of high-quality bio-oil for power generation
260 or to produce phenolic-based chemicals.

261 The slow lignin decomposition explains the low additional oxygen re-
262 duction (about 6%) of the samples treated at 400 °C compared with those
263 treated at 300 °C. There is an increase in the mass-loss rate from 400 until
264 550 °C, in accordance with the DTG curves (Fig. 3) and hence it observed a
265 small increment in oxygen reduction (9%) was observed between the samples
266 treated at 400 and 500 °C.

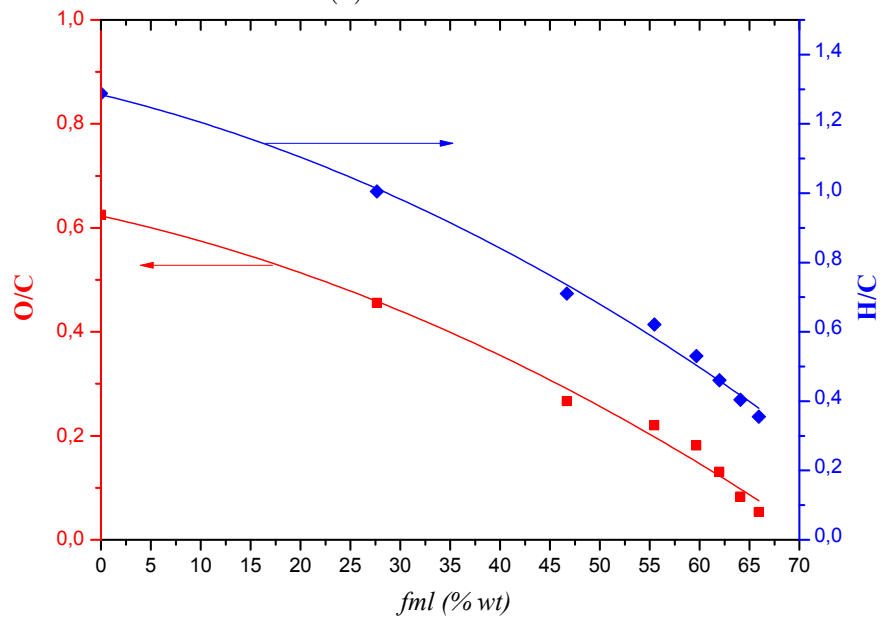
267 For the higher thermal treatment of 550 °C, 85.7% of the initial oxygen
268 content has been removed with just 71% of *fml*. It is not trivial to predict
269 the chemical structure of the 6% of oxygen that remains, which should be
270 highly aromatic considering its carbon enrichment. More explanations about
271 the chemical structure of carbonized charcoal can be found in [9].

272 Charcoal could be used as a reductant, in the production of chemicals,
273 refining of metals, production of activated carbon or just as domestic cooking
274 and heating [44]. The quality of the charcoals depends on the end use.
275 The yields of charcoal obtained in our standard experiment seem promising
276 because the treatment is almost uniform and leads to optimum yields [45, 46].

277 The van Krevelen diagram demonstrates the energy intensification with



(a)



(b)

Figure 4: (a) van Krevelen plot. (b) O/C and H/C ratios as function of the fml .

278 a linear correlation, $H/C \approx 1.64 (O/C) + 0.26$ ($R^2 = 0.999$), see Fig. 4a.
279 Elementary composition resembles a peat for the treatment at 250 °C and
280 from 300 °C it goes from characteristic charcoal towards anthracite at the
281 higher temperature [47, 48].

282 Furthermore, Fig. 4b shows a decrease of O/C and H/C ratios as a
283 function of fml . A good polynomial approximation can be found for both
284 ratios: $O/C \approx 0.62 - 4 \times 10^{-3}(fml) - 6.18 \times 10^{-5}(fml)^2$ with $R^2 = 0.986$
285 and $H/C \approx 1.28 - 7 \times 10^{-3}(fml) - 1.02 \times 10^{-4}(fml)^2$ with $R^2 = 0.993$.
286 These results show potential feasible application of the charcoals for electric
287 power generation, for example, via biomass integrated gasification gas turbine
288 (BIG/GT) technologies [44, 49], that could compete with fossil fuels, also
289 fewer emission and gas cleaning problems (from its lower nitrogen, sulfur
290 and ash contents) are expected.

291 Physicochemical properties such oxidation stability and moisture sorption
292 capacity can be predicted from the H/C and O/C ratios. Indeed, a consid-
293 erable reduction in the number of polar sites from the O/C ratio reduction
294 is expected and therefore a lower hygroscopicity in such chars. In [50], it
295 was proposed for a first time a parameter “Z”, ($Z = 2(O/C) - (H/C)$) to
296 computed the average carbon oxidation state. The Z values computed as in
297 [50], displays negative values for all chars here, in agreement with a reduced
298 states of carbon (lignin is most reduced), which has a pronounced effect on
299 its chemical reactivity.

300 3.3. Surface area and pore size analysis

301 Table 2 also displays the specific BET surface area and pore volume for
302 the untreated and char samples. The untreated and char, obtained up to 400
303 °C, had very low surface areas, lower than $0.6 m^2/g$, and a total pore volume
304 lower than $0.52 \times 10^{-3} cc/g$. This behavior is explained by considering the
305 high lignin content in the coconut endocarp, which could obstruct the pores
306 since alkali lignin pyrolysis displayed a melting even at low temperatures of
307 250 °C [24, 51], resulting in low surface area until 350 °C, where the primary
308 devolatilization process is less pronounced.

309 The low surface area of 400 °C-char could be attributed to coke formation
310 as a consequence of tar cracking by the secondary heterogeneously reactions
311 [52, 53], which may occur even in the pores of the particles [17]. Others
312 authors [9] also justify the low surface area for carbonized charcoal of melt
313 carbons (at 950 °C) as consequence of this liquid phase occurring during py-
314 rolysis. The 450 °C-char exhibits an exponential increase in the surface area,

315 reaching a value of $216 \text{ m}^2/\text{g}$ and total pore volume of 0.089 cc/g for the
 316 higher thermal treatment of $550 \text{ }^\circ\text{C}$, which represents an increment of more
 317 than a thousand times the untreated sample.

318 Coconut endocarp presented typical adsorption isotherm type II (Fig.
 319 5a), in accordance with the Brunauer classifications. In addition, char ob-
 320 tained until $400 \text{ }^\circ\text{C}$ showed the same type II isotherms, but less pronounced
 321 than those that were left untreated. From $450 \text{ }^\circ\text{C}$, the adsorption isotherms
 322 change from Type II to Type I, characteristic of microporous materials, with
 323 at least 80% of total pore volume adsorbed ($\approx 2.56 \times 10^{-3} \text{ cc/g}$) corresponding
 324 to microporous volume ($\approx 2.06 \times 10^{-3} \text{ cc/g}$).

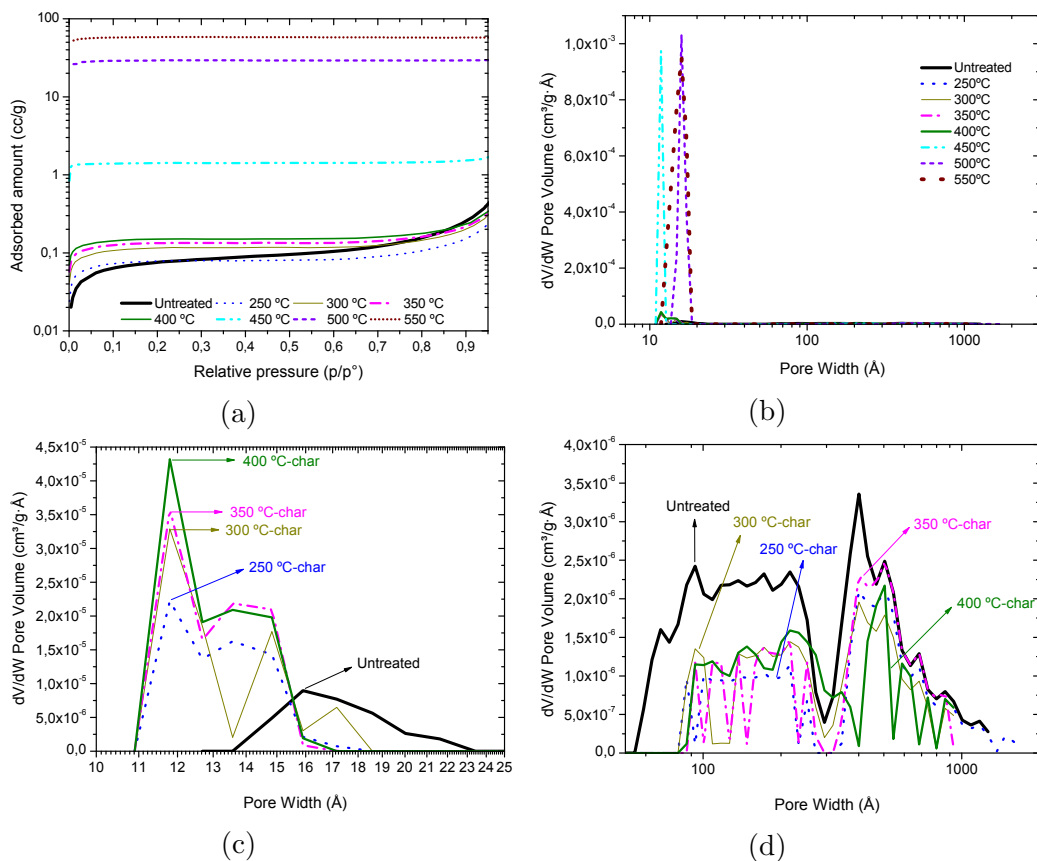


Figure 5: (a) Adsorption isotherms for the untreated and treated samples. (b) Pore size distribution (PSD) by Density functional theory (DFT) for untreated and treated samples (Below). (c) Amplification of PSD for the untreated and chars treated until $400 \text{ }^\circ\text{C}$, from 10 to 15 Å, and (d) from 25 until 200 Å.

325 Furthermore, the pore size distribution (PSD) in the chars, Fig. 5b,
326 shows that the exponential increment in the surface area is a consequence
327 of the micropore development, with a pore width between 10 and 20 Å. To
328 put this value in perspective, the diameter of the glucose molecule is 80 Å.
329 Considering the microfibrils are composed of many chain of cellulose, the
330 diameter of the microfibrils is more than 500 Å.

331 A zoom of the PSD for untreated and char samples until 400 °C, is pre-
332 sented in Fig. 5c and 5d. Although these samples are not microporous, the
333 small peaks detected between 10-25 Å of the pore width, match with the
334 size of micro-voids naturally presented in the cell walls of cellulose samples
335 [54], which apparently suffers a little contraction with thermal treatment. In
336 addition, peaks were detected in the range corresponding to mesoporous and
337 macroporous materials (Fig. 5d), with reduced intensity as a consequence
338 of the thermal treatment until reaching 400 °C. These peaks, detected be-
339 tween 100-2000 Å of pore width, could represent simple pores, presented
340 naturally in the scleroids cell walls and as will be seen later in the results of
341 the SEM/FEG micrographs.

342 From its microporous structure, surface area and carbon content, the 500
343 °C-char and 550 °C-char are proposed as a raw material for activated carbon
344 or syngas production from the gasification process, due to its expected more
345 uniform gas transfer, which should maintain the gasification reactivity with
346 elapsed time [55].

347 Finally, these results clearly show that the coconut endocarp undergoes
348 chemical changes as a consequence of the primary decomposition, but not
349 major changes in the porous structure until 450 °C.

350 3.4. ESEM and SEM-FEG visualization

351 Morphological changes of a single particle, as a consequence of the lower
352 (250 °C) and higher (550 °C) temperature of treatment, are displayed in
353 Figure 6. Simple pores, of about 1 μm of pore width, naturally present in
354 cell walls, are observed in the untreated samples. It is possible to observe
355 that the initial physical shape of the cell wall remains, even for the more
356 intense treatments at 550 °C (Fig. 6d), but with a significant contraction
357 in the structure of the sample, which is apparently submerged in a molten
358 fibrous mass.

359 Figure 7 illustrate the SEM/FEG micrographs for untreated and char
360 samples, obtained at 250 °C, 350 °C, and 550 °C. Apparently, an initial
361 softening in the chars treated at 250 °C and 350 °C, is observed (Fig. 7b and

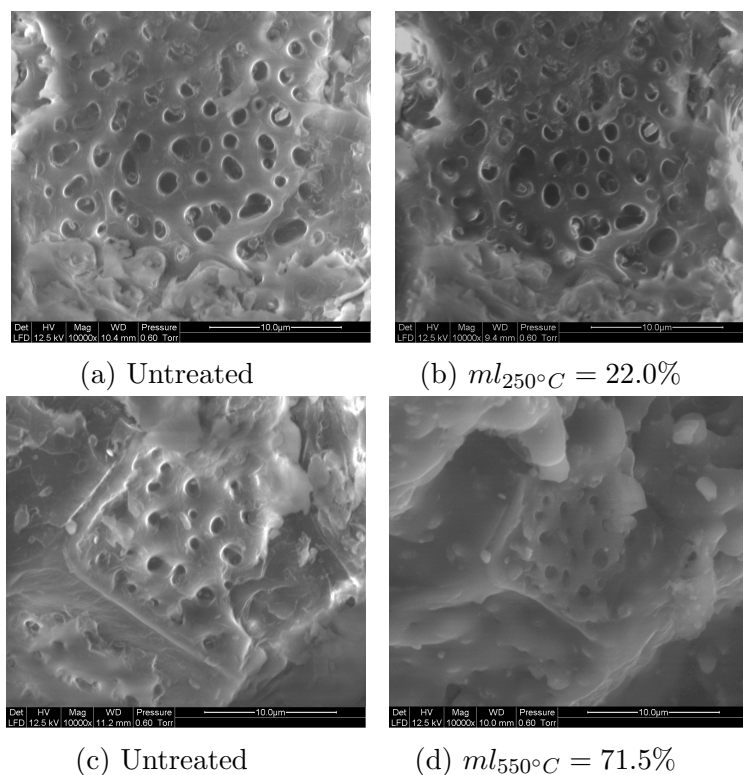


Figure 6: Morphological and structural changes over a single particle for the lower (a-b) and higher (c-d) temperature of treatment.

362 7c). As the intensity of treatment increases, the 550 °C-char appears to melt
 363 as displayed in the Figure 7d. These results are consistent with observations
 364 in lignin chars obtained in the same range of temperatures [24] and allow us
 365 to suppose that the low surface areas in the chars until 400 °C, could be a
 366 consequence of this softening.

367 Other SEM/FEG visualizations, not displayed here, allowed us to see
 368 the fibrous structure of the cell walls, which are composed of sclereid cells
 369 [2, 15]. The sclereids appear as columnar cells, with about 20 μm of diameter
 370 and variable depth. The longest dimension of the fiber bundle was difficult
 371 to define, but it was possible to observe that the fiber was longer than 50
 372 μm , with a thickness higher than 500 Å, which is in agreement with the
 373 microfibrils diameter.

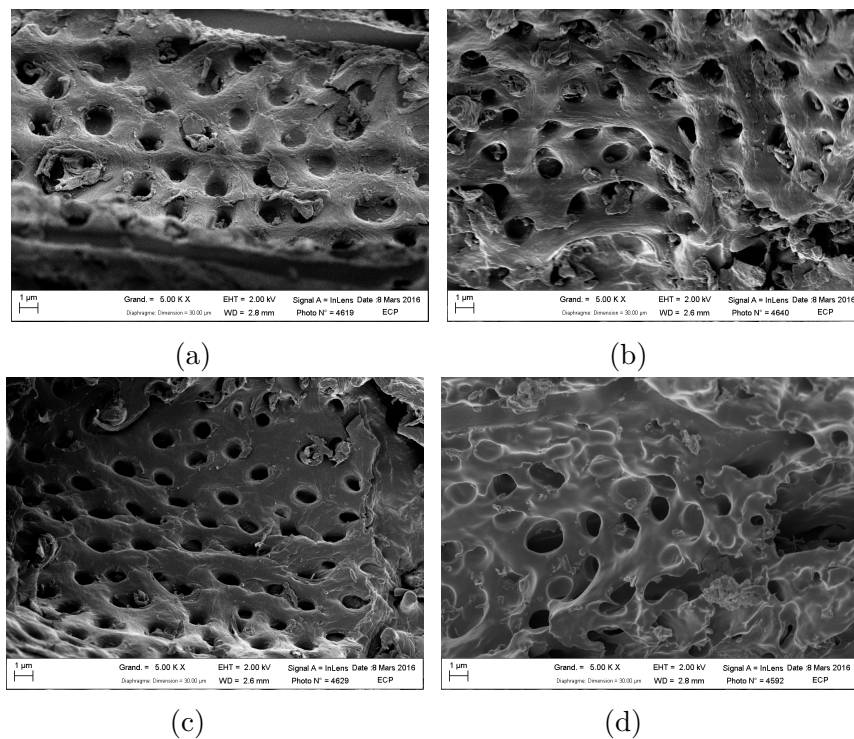


Figure 7: SEM/FEG micrographs of (a) coconut endocarp and its chars obtaining at (b) 250 °C, (c) 350 °C and (d) 550 °C.

374 3.5. Dynamic vapor sorption isotherms

375 An important factor in the moisture sorption properties of polymers is the
 376 hydroxyl groups (OH) accessibility, termed as sorption sites, because these
 377 OH-groups have strong hydrogen bond-interaction with water molecules.

378 Although cellulose has many OH-groups, only 33% of these are accessi-
 379 ble, whereas the surface of the microfibrils are considered sorption sites [56].
 380 Estimation of these sorption sites in wood, based on the molecular mass of
 381 its main components, had a very high water-accessible OH concentration for
 382 Xylan and Glucomannan [56] in comparison with cellulose and lignin con-
 383 centrations.

384 Figure 8 shows the sorption isotherms for the coconut endocarp and chars
 385 samples. It should be noted that the EMC in the coconut endocarp was lower
 386 than the typical values presented for wood samples [11, 12, 26, 57]. The
 387 coconut endocarp also contains about 53% of holocellulose [41], of which less
 388 than 22% is hemicellulose from the *fml* and DTG of the 250 °C-char. These

389 results are presented in Table 2 and Fig. 3. Its composition, together with
 390 the random distribution of its highly lignified sclereids cells [2], is responsible
 391 for its natural, more hydrophobic character, which explain its low values of
 392 EMC. In all cases, charring resulted in a decrease of the average EMC.

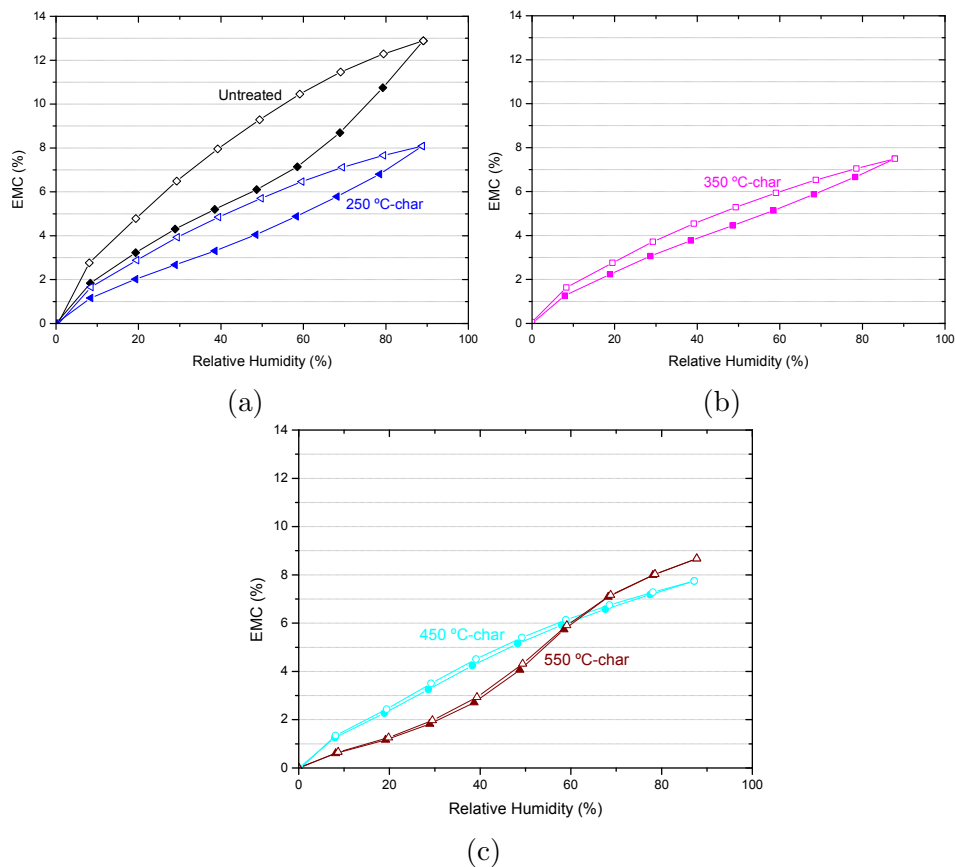


Figure 8: Dynamic vapor sorption isotherms for: (a) untreated and 250 °C-char, (b) 350 °C-char, (c) 450 °C-char and 550 °C-char.

393 It is also possible to observe the changes in the isotherm shape during
 394 pyrolysis. Typical sigmoidal type II curves for cellulosic materials are pre-
 395 sented. Both the untreated sample (Fig. 8a) and 250 °C-char exhibit this
 396 sigmoid shape as a result of their cellulose content and based on the fact that
 397 hemicellulose was decomposed at this temperature (Fig. 3). The isotherms
 398 going through a combination of type I and type II for 350 °C-char (Fig. 8b),
 399 because no more cellulose remains and, as expected, there is a higher lignin

400 fraction (Fig. 3) and do not show a microporous structure, unlike the 450
401 °C-char which exhibits the characteristic type I isotherm (Fig. 8c).

402 The pronounced curve type V for the char obtained at 550 °C (Fig. 8c)
403 is explained by its higher carbon content of about 86%. The charcoal has a
404 particular water adsorption behavior, which was already explained by [58].
405 This behavior is considered an initial weak uni-molecular attraction between
406 the carbon-water molecules at low RH values. As soon as the water molecules
407 become adsorbed and the RH increases, the next strongest interaction be-
408 tween water molecules happens more easily within the micro-voids until they
409 are filled.

410 At relative humidity values higher than 60% RH, the EMC for the 550
411 °C-char increases with respect to the 450 °C-char; this is a consequence of its
412 high microvoids number (Fig. 8c). The micro-porous volume is indicative of
413 the micro-void quantities present in the charcoal structure which, for the 550
414 °C-char, is forty times more than that for 450 °C-char. Then, the isotherm
415 type V would be in effect a type I isotherm, considering its microporous
416 structure, which matches with our previous results of N_2 type I adsorption
417 isotherms.

418 Similar sorption behaviors were obtained for torrefied and charcoal wood
419 up to 450 °C [12, 11, 59], but with different holding times at each peak
420 temperature.

421 Figure 9 shows that absolute hysteresis decreases as the pyrolysis intensity
422 increases; this is a consequence of overall decreases on the hygroscopicity. The
423 higher value of 3.32% was found in coconut endocarp at 60% RH.

424 The hysteresis ratio agreed with the results obtained in the mild thermal
425 treatment of wood [57]. The small increases in hysteresis ratio is explained
426 by the authors as a product of the stiffness increases with the higher times
427 of treatment.

428 The pore geometry has influence over the hysteresis, thus capillary con-
429 densation in mesopores with narrow necks and wide bodies could occur, in
430 the multilayer adsorption range or in micropores with narrow slip-like pores
431 materials [60]. A hysteresis model has been proposed in [13] as result of
432 different states (expansion and collapse of nanoporous in the cell-walls ma-
433 trix) of the material in which the adsorption and desorption process will take
434 place.

435 The microcapillaries or microvoids measure a diameter of 2-10 nm in wood
436 samples [54]. The pore size distribution shown in Fig. 5c, for the untreated
437 and chars until 400 °C, match this range. The desorption process takes place

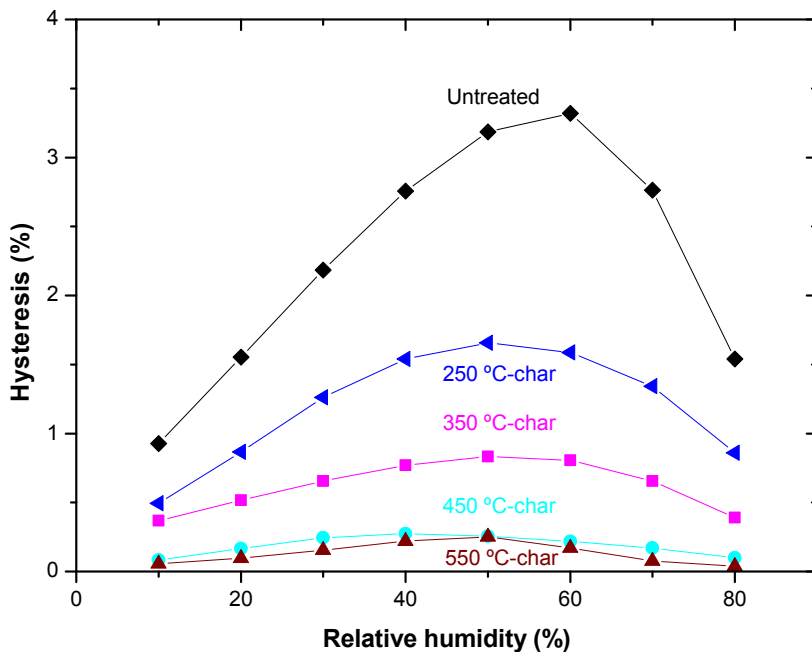


Figure 9: Absolute hysteresis of coconut endocarp and its chars at 0-90 % of RH.

438 in a swelling matrix, resulting from the hydrogen-bonds and hemicellulose,
 439 within the microcapillaries. A pore collapse could occur during the desorp-
 440 tion process for an untreated sample.

441 Similarly, hysteresis in 250 °C-char and 350 °C-char is explained by the
 442 water retention inside the collapse matrix, which will be less due at the
 443 lower sorption sites in cellulose. The lignin content could present a higher
 444 deformation facility to accomodate water, so, we expect that in the desorp-
 445 tion process, its deformation capacity could avoid the matrix collapse, thus
 446 reducing the hysteresis.

447 Char obtained at 450 °C and 550 °C present with negligible hysteresis.
 448 Both, have significant microporosity, which was confirmed by the exponential
 449 increases in the surface area BET and the pore size distribution (Table 2 and
 450 Fig. 5b). Microporous charcoals from different feedstock show hysteresis [9]
 451 for nitrogen adsorption, which was explained to be the result of pore shape,
 452 like narrow slit-shaped pores, that impede the diffusion of adsorbate [61].
 453 Also, microporous activated carbon shown a significantly high hysteresis as
 454 consequence of its functional groups, which increases the interaction with the

455 water molecules [62].

456 Recently, the loss of hysteresis for charcoal of wood was explained as
457 consequence of inaccessible internal porosity or negligible micropore forma-
458 tion which consequently increases in stiffness that avoids the micropore crea-
459 tion/destruction mechanism [12]. We wish to suggest an alternative expla-
460 nation. Given sufficient time, water will enter pores smaller than 4-5 Å with
461 dimensions comparable to that of the water molecules [63]. The lack of hys-
462 teresis in these two charcoals is most likely related to diffusional aspects. For
463 example, as a consequence of the geometrical pore shape that is more suit-
464 able to the mechanism of egress of water molecules; and the poor interaction
465 between the water molecules and the substrate, which facilitates its release
466 during the desorption process.

467 4. Conclusion

468 Prior work emphasized the enormous potential of coconut endocarp as
469 raw material to produce biofuel, charcoal or activated carbon. However, these
470 studies were not focused on its physicochemical evolution along the thermal
471 decomposition. In the present work, different analytical methods were used
472 to assess the product alterations due to pyrolysis: elemental analysis, surface
473 area and pore size analyses, ESEM and SEM/FEG observation and dynamic
474 vapor sorption determination.

475 At low temperature, the main effect is on the oxygen content, with a grad-
476 ual shift from native biomass to charcoal, which is preferable as solid fuel or
477 as feedstock to high-quality bio-oil. DTG curves indicate that the product
478 becomes lignin-like from a thermal treatment at 300 °C. At higher tempera-
479 ture, this trend continues, shifting towards fixed carbon and above 450 °C,
480 the chars acquire microporous materials characteristics with an exponential
481 increase of the specific surface and low hygroscopicity values. This allows
482 such treated products to be considered as raw materials in a gasification
483 process to produce syngas or activated carbon.

484 In addition, we proposed expressions for O/C and H/C ratios as a function
485 of the mass loss that can be used for prediction purposes. To our knowledge,
486 this is the first investigation of the sorption properties, BET surface area and
487 morphology evolution along the thermal decomposition of coconut endocarp
488 —*Acrocomia aculeata*—.

489 Our results provide sufficient evidence for the long-term application of
490 this feedstock and its chars as solid fuel or raw material in the gasification

491 process. However, the combustion characteristics and gasification conditions
492 still need be tested.

493

494 **Acknowledgment**

495

496 The authors thank Nathalie Ruscassier for assistance with SEM/FEG,
497 Mathilde Charters and Gonalo de Bastos Monteiro for help with surface area
498 BET analysis. S. Duarte thanks the support of CONACYT under grant Code
499 Project 14-INV-087. Financial supports from Grand Reims, the Marne de-
500 partment and the Grand Est region are gratefully acknowledged.

501

502 **References**

- 503 [1] A. B. Evaristo, J. A. S. Grossi, A. d. C. O. Carneiro, L. D. Pimentel,
504 S. Y. Motoike, K. N. Kuki, Actual and putative potentials of macauba
505 palm as feedstock for solid biofuel production from residues, *Biomass*
506 and *Bioenergy* 85 (2016) 18–24.
- 507 [2] S. B. Reis, M. O. Mercadante-Simes, L. M. Ribeiro, Pericarp develop-
508 ment in the macaw palm *Acrocomia aculeata* (arecaceae), *Rodrigusia* 63
509 (2012) 541–549.
- 510 [3] M. Plath, C. Moser, R. Bailis, P. Brandt, H. Hirsch, A.-M. Klein,
511 D. Walmsley, H. von Wehrden, A novel bioenergy feedstock in Latin
512 America? Cultivation potential of *Acrocomia aculeata* under current
513 and future climate conditions, *Biomass and Bioenergy* 91 (2016) 186 –
514 195.
- 515 [4] G. Ciconini, S. Favaro, R. Roscoe, C. Miranda, C. Tapeti, M. Miyahira,
516 L. Bearari, F. Galvani, A. Borsato, L. Colnago, M. Naka, Biometry
517 and oil contents of *Acrocomia aculeata* fruits from the Cerrados and
518 Pantanal biomes in Mato Grosso do Sul, Brazil, *Industrial Crops and*
519 *Products* 45 (2013) 208 – 214.
- 520 [5] I. Gauto, R. E. Spichiger, F. W. Stauffer, Diversity, distribution and
521 conservation status assessment of Paraguayan palms (Arecaceae), *Bio-*
522 *diversity and Conservation* 20 (2011) 2705–2728.
- 523 [6] J. Poetsch, D. Hauptenthal, I. Lewandowski, D. Oberländer, T. Hilger,
524 *Acrocomia aculeata* sustainable oil crop, *Rural* 21 (2012) 41–44.

- 525 [7] S. J. Duarte, J. Lin, D. Alviso, J. C. Rolón, Effect of Temperature
526 and Particle Size on the Yield of Bio-oil, Produced from Conventional
527 Coconut Core Pyrolysis, *International Journal of Chemical Engineering
528 and Applications* 7 (2016) 102–108.
- 529 [8] K. Mochidzuki, F. Soutric, K. Tadokoro, M. J. Antal, M. Tóth, B. Zelei,
530 G. Várhegyi, Electrical and physical properties of carbonized charcoals,
531 *Industrial & Engineering Chemistry Research* 42 (2003) 5140–5151.
- 532 [9] J. Bourke, M. Manley-Harris, C. Fushimi, K. Dowaki, T. Nunoura, M. J.
533 Antal, Do all carbonized charcoals have the same chemical structure?
534 2. A model of the chemical structure of carbonized charcoal, *Industrial
535 & Engineering Chemistry Research* 46 (2007) 5954–5967.
- 536 [10] M. Keiluweit, P. S. Nico, M. G. Johnson, M. Kleber, Dynamic molecular
537 structure of plant biomass-derived black carbon (biochar), *Environmental
538 Science & Technology* 44 (2010) 1247–1253.
- 539 [11] C.-M. Popescu, C. A. Hill, R. Anthony, G. Ormondroyd, S. Curling,
540 Equilibrium and dynamic vapour water sorption properties of biochar
541 derived from apple wood, *Polymer Degradation and Stability* 111 (2015)
542 263–268.
- 543 [12] M. Kymäläinen, L. Rautkari, C. A. S. Hill, Sorption behaviour of tor-
544 refied wood and charcoal determined by dynamic vapour sorption, *Jour-
545 nal of Materials Science* 50 (2015) 7673–7680.
- 546 [13] C. A. S. Hill, A. Norton, G. Newman, The water vapor sorption behavior
547 of natural fibers, *Journal of Applied Polymer Science* 112 (2009) 1524–
548 1537.
- 549 [14] W. Willems, The water vapor sorption mechanism and its hysteresis in
550 wood: the water/void mixture postulate, *Wood Science and Technology*
551 48 (2014) 499–518.
- 552 [15] H. C. Mazzottini-dos Santos, L. M. Ribeiro, M. O. Mercadante-Simões,
553 B. F. Sant’Anna-Santos, Ontogenesis of the pseudomonomerous fruits
554 of *Acrocomia aculeata* (Arecaceae): a new approach to the development
555 of pyrenarium fruits, *Trees* 29 (2015) 199–214.

- 556 [16] T. J. Hilbers, Z. Wang, B. Pecha, R. J. Westerhof, S. R. Kersten, M. R.
557 Pelaez-Samaniego, M. Garcia-Perez, Cellulose-lignin interactions during
558 slow and fast pyrolysis, *Journal of Analytical and Applied Pyrolysis* 114
559 (2015) 197 – 207.
- 560 [17] C. D. Blasi, Modeling chemical and physical processes of wood and
561 biomass pyrolysis, *Progress in Energy and Combustion Science* 34 (2008)
562 47 – 90.
- 563 [18] C. D. Blasi, Numerical simulation of cellulose pyrolysis, *Biomass and*
564 *Bioenergy* 7 (1994) 87 – 98.
- 565 [19] E. Bohn, Tablero de comando para la promoción de los biocombustibles
566 en Paraguay, Technical Report, Naciones Unidas Comisión Económica
567 para América Latina y el Caribe (CEPAL), 2009.
- 568 [20] G. Almeida, J. Brito, P. Perré, Alterations in energy properties of euca-
569 lyptus wood and bark subjected to torrefaction: The potential of mass
570 loss as a synthetic indicator, *Bioresource Technology* 101 (2010) 9778 –
571 9784.
- 572 [21] C. Couhert, J.-M. Commandre, S. Salvador, Is it possible to predict
573 gas yields of any biomass after rapid pyrolysis at high temperature from
574 its composition in cellulose, hemicellulose and lignin?, *Fuel* 88 (2009)
575 408–417.
- 576 [22] A. Gani, I. Naruse, Effect of cellulose and lignin content on pyrolysis
577 and combustion characteristics for several types of biomass, *Renewable*
578 *Energy* 32 (2007) 649–661.
- 579 [23] D. Lv, M. Xu, X. Liu, Z. Zhan, Z. Li, H. Yao, Effect of cellulose,
580 lignin, alkali and alkaline earth metallic species on biomass pyrolysis
581 and gasification, *Fuel Processing Technology* 91 (2010) 903–909.
- 582 [24] R. K. Sharma, J. B. Wooten, V. L. Baliga, X. Lin, W. G. Chan, M. R.
583 Hajaligol, Characterization of chars from pyrolysis of lignin, *Fuel* 83
584 (2004) 1469–1482.
- 585 [25] C. A. S. Hill, A. J. Norton, G. Newman, The water vapour sorption
586 properties of sitka spruce determined using a dynamic vapour sorption
587 apparatus, *Wood Science and Technology* 44 (2010) 497–514.

- 588 [26] C. A. S. Hill, J. Ramsay, B. Keating, K. Laine, L. Rautkari, M. Hughes,
589 B. Constant, The water vapour sorption properties of thermally modified
590 and densified wood, *Journal of Materials Science* 47 (2012) 3191–3197.
- 591 [27] J. Wannapeera, B. Fungtammasan, N. Worasuwannarak, Effects of tem-
592 perature and holding time during torrefaction on the pyrolysis behaviors
593 of woody biomass, *Journal of Analytical and Applied Pyrolysis* 92 (2011)
594 99 – 105.
- 595 [28] M. J. Prins, K. J. Ptasinski, F. J. Janssen, Torrefaction of wood: Part
596 2. analysis of products, *Journal of Analytical and Applied Pyrolysis* 77
597 (2006) 35 – 40.
- 598 [29] A. G. Bradbury, Y. Sakai, F. Shafizadeh, A kinetic model for pyrolysis
599 of cellulose, *Journal of Applied Polymer Science* 23 (1979) 3271–3280.
- 600 [30] J. Piskorz, D. S. A. Radlein, D. S. Scott, S. Czernik, Pretreatment of
601 wood and cellulose for production of sugars by fast pyrolysis, *Journal*
602 *of Analytical and Applied Pyrolysis* 16 (1989) 127–142.
- 603 [31] J. L. Banyasz, S. Li, J. L. Lyons-Hart, K. H. Shafer, Cellulose pyrolysis:
604 the kinetics of hydroxyacetaldehyde evolution, *Journal of Analytical*
605 *and Applied Pyrolysis* 57 (2001) 223–248.
- 606 [32] E. Jakab, Chapter 3 - Analytical Techniques as a Tool to Understand
607 the Reaction Mechanism, in: A. Pandey, T. Bhaskar, M. Stcker, R. K.
608 Sukumaran (Eds.), *Recent Advances in Thermo-Chemical Conversion*
609 *of Biomass*, Elsevier, Boston, 2015, pp. 75 – 108.
- 610 [33] P. Lv, G. Almeida, P. Perré, TGA-FTIR Analysis of Torrefaction of
611 Lignocellulosic Components (cellulose, xylan, lignin) in Isothermal Con-
612 ditions over a Wide Range of Time Durations, *BioResources* 10 (2015)
613 4239–4251.
- 614 [34] H. Yang, R. Yan, H. Chen, D. H. Lee, C. Zheng, Characteristics of
615 hemicellulose, cellulose and lignin pyrolysis, *Fuel* 86 (2007) 1781–1788.
- 616 [35] A. E. Harman-Ware, M. Crocker, R. B. Pace, A. Placido, S. Morton III,
617 S. DeBolt, Characterization of endocarp biomass and extracted lignin
618 using pyrolysis and spectroscopic methods, *BioEnergy Research* 8 (2015)
619 350–368.

- 620 [36] V. Mendu, A. E. Harman-Ware, M. Crocker, J. Jae, J. Stork, S. Morton,
621 A. Placido, G. Huber, S. DeBolt, Identification and thermochemical
622 analysis of high-lignin feedstocks for biofuel and biochemical production,
623 *Biotechnology for biofuels* 4 (2011) 43.
- 624 [37] J. Ralph, Hydroxycinnamates in lignification, *Phytochemistry Reviews*
625 9 (2010) 65–83.
- 626 [38] J. Rencoret, J. Ralph, G. Marques, A. Gutierrez, A. T. Martínez, J. C.
627 del Rio, Structural characterization of lignin isolated from coconut (co-
628 cos nucifera) coir fibers, *Journal of agricultural and food chemistry* 61
629 (2013) 2434–2445.
- 630 [39] P. H. G. Cademartori, P. S. d. Santos, L. Serrano, J. Labidi, D. A.
631 Gatto, Effect of thermal treatment on physicochemical properties of
632 gympie messmate wood, *Industrial Crops and Products* 45 (2013) 360–
633 366.
- 634 [40] T. Sonobe, N. Worasuwanarak, Kinetic analyses of biomass pyrolysis
635 using the distributed activation energy model, *Fuel* 87 (2008) 414–421.
- 636 [41] J. d. C. Silva, L. E. G. Barrichelo, J. O. Brito, Endocarpos de babaçu
637 e de macaúba comparados à madeira de eucalyptus grandis para a
638 produção de carvão vegetal, *Ipef* 34 (1986) 31–34.
- 639 [42] M. I. Al-Wabel, A. Al-Omran, A. H. El-Naggar, M. Nadeem, A. R.
640 Usman, Pyrolysis temperature induced changes in characteristics and
641 chemical composition of biochar produced from conocarpus wastes,
642 *Bioresource technology* 131 (2013) 374–379.
- 643 [43] S. Yaman, Pyrolysis of biomass to produce fuels and chemical feedstocks,
644 *Energy conversion and management* 45 (2004) 651–671.
- 645 [44] M. J. Antal, E. Croiset, X. Dai, C. DeAlmeida, W. S.-L. Mok, N. Nor-
646 berg, J.-R. Richard, M. Al Majthoub, High-yield biomass charcoal,
647 *Energy & Fuels* 10 (1996) 652–658.
- 648 [45] L. Wang, M. Trninic, Ø. Skreiberg, M. Gronli, R. Considine, M. J.
649 Antal Jr, Is elevated pressure required to achieve a high fixed-carbon
650 yield of charcoal from biomass? part 1: Round-robin results for three
651 different corncob materials, *Energy & Fuels* 25 (2011) 3251–3265.

- 652 [46] L. Wang, Ø. Skreiberg, M. Gronli, G. P. Specht, M. J. Antal Jr, Is ele-
653 vated pressure required to achieve a high fixed-carbon yield of charcoal
654 from biomass? part 2: The importance of particle size, *Energy & Fuels*
655 27 (2013) 2146–2156.
- 656 [47] J. J. Chew, V. Doshi, Recent advances in biomass pretreatment–
657 torrefaction fundamentals and technology, *Renewable and Sustainable*
658 *Energy Reviews* 15 (2011) 4212–4222.
- 659 [48] S. Cavagnol, J. F. Roesler, E. Sanz, W. Nastoll, P. Lu, P. Perré, Exother-
660 micity in wood torrefaction and its impact on product mass yields: From
661 micro to pilot scale, *The Canadian Journal of Chemical Engineering* 93
662 (2015) 331–339.
- 663 [49] P. McKendry, Energy production from biomass (part 2): conversion
664 technologies, *Bioresource technology* 83 (2002) 47–54.
- 665 [50] W. Willems, C. Mai, H. Militz, Thermal wood modification chemistry
666 analysed using van krevelen’s representation, *International Wood Prod-*
667 *ucts Journal* 4 (2013) 166–171.
- 668 [51] V. Baliga, R. Sharma, D. Miser, T. McGrath, M. Hajaligol, Physical
669 characterization of pyrolyzed tobacco and tobacco components, *Journal*
670 *of Analytical and Applied Pyrolysis* 66 (2003) 191 – 215.
- 671 [52] Y. Zhang, S. Kajitani, M. Ashizawa, K. Miura, Peculiarities of rapid
672 pyrolysis of biomass covering medium-and high-temperature ranges, *En-*
673 *ergy & fuels* 20 (2006) 2705–2712.
- 674 [53] D. Dayton, A review of the literature on catalytic biomass tar destruc-
675 tion, US DOE NREL Report Golden, CO (2002) 510–32815.
- 676 [54] C. A. Hill, A. N. Papadopoulos, A review of methods used to determine
677 the size of the cell wall microvoids of wood, *Journal-Institute of Wood*
678 *Science* 15 (2001) 337–345.
- 679 [55] Q. Xu, S. Pang, T. Levi, Reaction kinetics and producer gas com-
680 positions of steam gasification of coal and biomass blend chars, part
681 1: Experimental investigation, *Chemical engineering science* 66 (2011)
682 2141–2148.

- 683 [56] E. T. Englund, L. G. Thygesen, S. Svensson, C. A. S. Hill, A critical
684 discussion of the physics of woodwater interactions, *Wood Science and*
685 *Technology* 47 (2013) 141–161.
- 686 [57] Z. Jalaludin, C. A. Hill, Y. Xie, H. W. Samsi, H. Husain, K. Awang, S. F.
687 Curling, Analysis of the water vapour sorption isotherms of thermally
688 modified acacia and sesendok, *Wood Material Science and Engineering*
689 5 (2010) 194–203.
- 690 [58] S. Brunauer, L. S. Deming, W. E. Deming, E. Teller, On a theory of the
691 van der waals adsorption of gases, *Journal of the American Chemical*
692 *Society* 62 (1940) 1723–1732.
- 693 [59] G. Almeida, J. O. Brito, P. Perre, Changes in wood-water relationship
694 due to heat treatment assessed on micro-samples of three eucalyptus
695 species, *Holzforschung* 63 (2009) 80–88.
- 696 [60] K. S. Sing, Reporting physisorption data for gas/solid systems with
697 special reference to the determination of surface area and porosity (rec-
698 ommendations 1984), *Pure and Applied Chemistry* 57 (1985) 603–619.
- 699 [61] W. Pattaraprakorn, R. Nakamura, T. Aida, H. Niiyama, Adsorption of
700 CO_2 and N_2 onto charcoal treated at different temperatures, *Journal of*
701 *Chemical Engineering of Japan* 38 (2005) 366–372.
- 702 [62] A. Harding, N. Foley, P. Norman, D. Francis, K. Thomas, Diffusion bar-
703 riers in the kinetics of water vapor adsorption/desorption on activated
704 carbons, *Langmuir* 14 (1998) 3858–3864.
- 705 [63] P. Lodewyckx, The effect of water uptake in ultramicropores on the
706 adsorption of water vapour in activated carbon, *Carbon* 48 (2010) 2549–
707 2553.